SORET AND DUFOUR EFFECTS ON Ag–TiO2/WATER IN A CASSON HYBRID NANOFLUID OVER A MOVING VERTICAL PLATE WITH CONVECTIVE BOUNDARY CONDITIONS

K. Fatima[1], J.L. Rama Prasad[2]*

1Department of Mathematics, Krishna University, Machilipatnam, AP, India
2Department of Mathematics, P.B. Siddhartha College of Arts & Science, Vijayawada, AP, India
Email: bukharizulfa@gmail.com
*Corresponding Author e-mail: jlrprasad@gmail.com

This research presents a comprehensive investigation of the Soret and Dufour effects on Casson hybrid nanofluid (HNF) flow past a moving vertical plate, with silver (Ag) and titanium dioxide (TiO2) nanoparticles dispersed in water. The incorporation of Ag–TiO2 hybrid nanoparticles combines the exceptional thermal conductivity of silver with the chemical stability and cost-effectiveness of TiO2, creating a fluid with superior transport properties compared to conventional single-component nanofluids. The governing partial differential equations describing momentum, heat and mass transfer are transformed into a set of nonlinear ordinary differential equations using similarity transformations. These equations are solved numerically via the Keller Box method, ensuring stability and accuracy in handling coupled highly nonlinear systems. In addition, an analysis was performed to examine the influence of nanoparticle morphology on velocity, temperature and concentration distributions, thereby validating and enriching the numerical outcomes. The results reveal that variable nanoparticle morphology and the combined Ag–TiO2 dispersion significantly enhance heat transfer rates and mass transfer rates while reducing frictional losses near the plate surface. The inclusion of Soret and Dufour effects further amplifies cross-coupling between thermal and solutal fields leading to improved transport efficiency. These findings not only provide new insights into Casson hybrid nanofluid dynamics but also highlight the critical role of cross-diffusion in optimizing heat and mass transfer systems. The integration of Casson fluid rheology, hybrid nanoparticles and cross-diffusion effects under realistic boundary conditions has direct implications for industrial cooling, metallurgical processing, biomedical drug delivery and energy system optimization. By demonstrating the synergistic performance of Ag–TiO2 nanofluids, this study establishes a pathway for designing next-generation thermal management and biomedical transport technologies.

Keywords: *Convective Boundary Conditions; MHD; Casson Hybrid Nanofluid; Shape of Nanoparticles; Soret and Dufour effects*
PACS: 47.20.Bp, 44.40.+a,47.52.+j, 47.11.Bc

INTRODUCTION

The development of advanced heat-transfer fluids has become imperative as industries demand higher thermal management performance across applications ranging from electronic cooling and energy systems to biomedical devices and chemical processing. Nanofluids are base fluids loaded with suspended nanoparticles offer a promising route for enhancing thermal transport because the inclusion of high-conductivity particles increases the effective thermal conductivity of the mixture. More recently, hybrid nanofluid suspensions containing two or more distinct nanoparticle species have attracted attention because they combine complementary thermal, chemical and rheological attributes of different particles to yield superior heat-transfer and stability characteristics compared with single-component nanofluids. Among hybrid combinations, systems that pair noble metals (e.g., silver, Ag) with metal oxides (e.g., titanium dioxide, TiO2) are particularly attractive. Silver imparts exceptionally high thermal and electrical conductivity, while TiO2 contributes chemical stability, corrosion resistance and cost-effectiveness. The Ag–TiO2/water hybrid therefore represents a practical formulation for applications where both enhanced heat transfer and operational robustness are required. However, realistic performance prediction of such fluids requires more than bulk-averaged property estimates. It requires capturing the coupled interaction between momentum, heat and mass transport under operating conditions that often involve large temperature and concentration gradients.

The Casson fluid model, which characterizes yield-stress behavior and shear-thinning dynamics, is widely used to represent fluids whose microstructural deformation affects macroscopic flow examples include blood, polymeric suspensions, and certain high-viscosity industrial fluids. Combining Casson rheology with hybrid nanoparticle suspensions introduces rich, nonlinear coupling between flow resistance, particle transport and thermal behavior that cannot be captured by Newtonian assumptions. Therefore, investigations of Casson hybrid nanofluids are both theoretically significant and practically necessary.

When coupled heat and mass transfer occur, two cross-diffusion phenomena may become important. Soret effect induces mass flux i.e., particles or solutes migrate from hot to cold or vice versa, depending on species specifics. In practical terms, the Soret effect alters concentration fields in the presence of thermal gradients, thereby changing local thermophysical properties and feeding back on flow and heat transfer. Dufour effect induces a heat flux i.e., variations in species concentration drive thermal energy transport. Though often smaller than the direct conductive heat flux, the Dufour effect can modify temperature distributions in systems with strong concentration gradients or significant solutal fluxes.

The two effects are reciprocal manifestations of cross-coupled transport: Soret describes heat driving mass flux; Dufour describes mass flux driving heat. Their relative importance depends on fluid properties, particle size and concentration and the magnitudes of temperature and concentration gradients. In nanoparticle-laden systems especially hybrid formulations with differing particle diffusivities and thermal conductivities Soret and Dufour coupling can appreciably affect Nusselt and Sherwood numbers, boundary-layer structure, and ultimately system performance.

The literature on nanofluid heat and mass transfer is extensive, covering experimental measurements, empirical correlations for effective properties and numerous numerical investigations. Foundational models such as Buongiorno's two-component approach accounted for key microscale transport mechanisms (Brownian diffusion and thermophoresis), and many studies have extended these ideas to hybrid nanofluids, magnetic fields, viscous dissipation and slip conditions. However, several gaps and limitations remain. While there is growing work on hybrid nanofluids, relatively few studies integrate non-Newtonian Casson rheology with hybrid particle systems, particularly with combinations such as Ag–TiO₂ that present strong contrasts in conductivity and diffusivity. Although some investigations account for Soret/Dufour in Newtonian nanofluids or single-particle Casson fluids, the combined influence of both cross-effects in Casson hybrid nanofluids is underexplored. Given the differing particle mobilities and interaction potentials in hybrid suspensions, cross-diffusion coupling may be amplified or altered compared with single-component systems.

Numerical studies frequently assume idealized spherical particles and homogeneous dispersion yet particle morphology (e.g., platelets, rods, aggregates) and real dispersion quality critically affect effective thermal conductivity and viscosity. Experimental efforts that systematically examine the interplay of particle shape, hybrid mixing ratios and cross-diffusion under flowing conditions are limited. Many existing analyses focus on canonical problems do not combine moving boundaries, convective boundary conditions and mixed convection with non-Newtonian rheology conditions typical in industrial processes such as coating, extrusion, and vertical heat exchangers. There is a paucity of system-level analysis that quantifies the trade-off between enhanced heat transfer and increased pumping or process complexity specifically for Casson hybrid formulations with Soret/Dufour effects.

Abdul Aziz [1] derived similarity solution in laminar boundary layer flow over flat plate with convective surface. Yahyaee [2] explored how different nanoparticle shapes affect film boiling on vertical cylinders using numerical simulations. Azad Hussain et al. [3] investigated flow, heat transfer characteristics in magneto hydro dynamic bioconvective carbon nanotubes flow across stretched surface incorporating Dufour and Soret effects. Bhavanam Naga Lakshmi et al. [4] examined three-dimensional rotating HNF flow across linearly stretchable surface including Ag, CuO nano particles with H₂O as base fluid considering Soret, Dufour effects. Cebeci and Bradshaw [5] described Keller Box implicit finite difference system. RamReddy et al. [6] examined mixed convective heat, mass transport in semi-infinite vertical flat plate within nanofluid taking Soret effect into account. Chundru Maheswari [7] examined MHD hybrid nanofluid, namely MgO − Ag/H₂O in laminar and steady-state flow over a horizontally positioned thin needle that can move same or opposite direction to free stream, employing shooting method, taking into account thermophoresis parameter, Brownian motion effects. Eleni Seid et al. [8] conducted mathematical investigation of combined slip, Soret, Dufour effects in electrically conducting nanofluid flow across vertically extending sheet.

Isa et al. [9] analyzed water-based hybrid nanofluid, including alumina (Al2O3), copper (Cu) nanoparticles in two-dimensional mathematical model. Iskandar Waini [10] investigated consistent mixed convection flow along vertical porous surface containing hybrid nanoparticles. J. Jayaprakash et al. [11] elucidated Maxwell nanofluid flow across linearly stretched porous sheet accounting for interactions with mixed convection, Dufour, Soret numbers. Kavita Jat et al. [12] examined Soret and Dufour impacts on magnetohydrodynamic hybrid nanofluids across nonlinear stretched sheet. Balamurugan et al. [13] examined convective electrically conducting Newtonian fluid flow over inclined heated porous plate. Minea Alina [14] proposed numerical assessment on three oxide-based nanofluids and their hybrids. Mansour and Bakier [15] conducted an experiment on mixed convection heat, mass transfer utilizing finite difference approach within porous saturated cavity influenced by dual-moving lid and heat sources.

Sheikholeslami [16] studied nanoparticle shape effects in forced convective nanofluid in constant magnetic field. Sreedhar et al. [17] examined convective heat, mass transfer effects in wedge-shaped flows inside nanofluids. Veera Krishna et al. [18] studied radiative unsteady non-Newtonian Casson hybrid nanofluid across porous surface with infinite exponential acceleration, driven by slip velocity in rotating frame. Nor Alifah Rosaidi et al. [19] examined aligned magnetohydrodynamic nanofluid convective flow across plate moving vertically. Norsyasya Zahirah et al. [20] investigated nanoparticle influence morphologies on Casson hybrid nanofluid flow across moving vertical plate. Noreen and Adil [21] considered Cu–water nanofluid flow with different shaped nanoparticles. Zainal et al. [22] examined steady MHD stagnation point nanofluid flow along flat convective plate. P. Chandrakala [23] studied hybrid nanofluid flow across sheet that expands exponentially, using heat source, sink. Ruchi Jain et al. [24] investigated on Williamson hybrid fluid flow utilizing single, multi-wall carbon nanotubes combined with CuO and water examining effects of Hall effect, Soret, Dufour effect over porous stretching or shrinking lamina with suction, injection. Sahar Goudarzi et al. [25] examined how Brownian motion, thermophoresis affect nanoparticles movement in Ag-MgO/Water hybrid nanofluid. S.A.M. Mehryan et al. [26] examined Aluminium Oxide - Copper water nanofluid within free convective heat transport porous cavity. S. Hussain et al. [27] statistically explored entropy production resulting from partly heated square double lid-driven cavity filled with Aluminium Oxide -water nano fluid under inclined magnetic field. Anwar et al [28]

formulated two various fractional models to explain flow patterns, thermal behavior in sodium alginate (NaAlg/SA) based hybrid nanofluid. Khaleque [29] studied convective flow in mixed power-law fluid over continuously stretched surface.

This study examines Soret, Dufour effects on Casson hybrid nanofluid (Ag-TiO2/Water) in relation to moving vertical plate. Silver (Ag) and titanium dioxide (TiO2) were incorporated into water-based fluid for this study. Similarity transformation techniques are employed to translate PDE's into ODE's subsequently solved numerically using Keller Box method. This study also examines several nanoparticle geometries impact on velocity, temperature, concentration profiles. Furthermore, quantitative results are examined, tabulated, graphically represented considering various non-dimensional parameters. By analyzing the role of nanoparticle morphology and thermal conductivity, the study aims to provide insights into how hybrid nanofluids can be used for optimal performance in industrial applications.

MATHEMATICAL FORMULATION

Rheological formula for Casson hybrid nanofluids with isotropic and incompressible flow is:

$$\tau_{ij} = \begin{cases} (\mu_B + p_y/\sqrt{2\pi})2e_{ij} & , \pi > \pi_c \\ (\mu_B + p_y/\sqrt{2\pi_c})2e_{ij}, & \pi < \pi_c \end{cases}$$

where μ_B is non-Newtonian fluid's dynamic viscosity, p_y is yield stress, π_c is critical value based on non-Newtonian model, Plate is assumed to move at constant velocity $U_w = \lambda U_\infty$, where U_w, λ being plate velocity, its parameter respectively.

Aligned magnetic field with acute angle, α as shown in Figure 1 is applied to flow. It is recognized as origin function, expressed by $B(x) = \frac{B_0}{\sqrt{x}}$ with $B_0 \neq 0$.
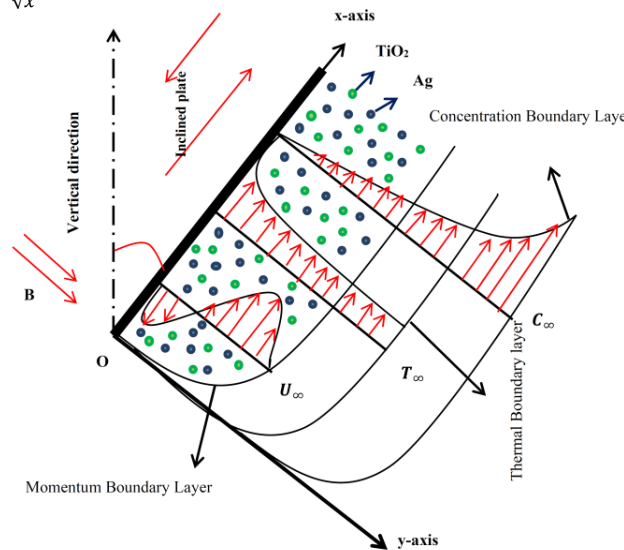

Figure 1. Physical model of Problem

Magnetic field intensity is denoted by B_0, (x,y) represents coordinates along plate. Assuming stable two-dimensional boundary layer flow, following governing equations developed as:

$$u_x + v_y = 0 \tag{1}$$

$$uu_x + vu_y = \frac{\mu_{hnf}}{\rho_{hnf}}(1+\frac{1}{\beta})\frac{\partial^2 u}{\partial y^2} + \frac{(\rho\beta)_{hnf}}{\rho_{hnf}}g(T-T_\infty) + \frac{(\rho\beta)_{hnf}}{\rho_{hnf}}g(C-C_\infty) - \frac{\sigma B_0^2(x)\sin^2\alpha(u-U_\infty)}{\rho_{hnf}} \tag{2}$$

$$uT_x + vT_y = \alpha_{hnf}T_{yy} - \frac{1}{(\rho C_p)}(q_r)_y + \tau\left[D_B C_y T_y + \frac{D_T}{T_\infty}(T_y)^2\right] + \frac{D_T K_T}{C_s C_p}C_{yy} \tag{3}$$

$$uC_x + vC_y = D_m C_{yy} + \frac{D_T K_T}{T_\infty}T_{yy} \tag{4}$$

Boundary conditions:

$$u = u_w = \lambda U_\infty, v = 0, k_{hnf} \frac{\partial T}{\partial y} = h_f \left(T - T_\infty \right), D_m \frac{\partial C}{\partial y} = h_m \left(C - C_\infty \right) at\, y = 0,$$

$$u \to 0, T \to T_\infty, C \to C_\infty \, as\, y \to \infty \tag{5}$$

where u, v indicates velocity components along x, y-axis, α is inclined magnetic field, T, T_f is the temperature of fluid, nanofluid, $U_\infty, T_\infty, C_\infty$ denotesfree stream velocity, temperature, concentration respectively. g is gravity, ρ_{hnf} is effective density, σ is electrical conductivity, $(\rho\beta)_{hnf}$ is thermal expansion coefficient, μ_{hnf} is effective dynamic viscosity, α_{hnf} is fluid's thermal diffusivity, $(\rho C_p)_{hnf}$ is fluid's heat capacity, k_{hnf} is thermal conductivity(hybrid nanofluids), M is magnetic parameter, h_f is heat transfer coefficient $\left(h_f = \frac{c}{\sqrt{x}}, c \text{ is a constant } \right)$, h_m is mass transfer coefficient of fluid, D_B is Brown dissemination coefficient, D_T is heat dispersion coefficient, D_m is mass diffusivity and β is the Casson hybrid nanofluid parameter.

Rosseland approximation for radiative heat flow $q_r = -\frac{4\sigma^*}{3k^*} \frac{\partial T^4}{\partial y}$ where (σ), k^* being Stefan-Boltzman constant, absorption coefficient respectively.

Considering temperature function as T^4 given by $T^4 \cong 4T_\infty^3 T - 3T_\infty^4$, the equation (3) becomes

$$u T_x + v T_y = \alpha T_{yy} - \frac{16\sigma T_\infty^3}{3(\rho C_p)_{hnf} k^*} T_{yy} + \tau \left[D_B C_y T_y + \frac{D_T}{T_\infty} (T_y)^2 \right] + \frac{D_T K_T}{C_s C_p} C_{yy} \tag{6}$$

Introducing stream function $\psi(x, y)$ as shown below

$$u = \frac{\partial \psi}{\partial y}, v = -\frac{\partial \psi}{\partial x}$$

Following similarity variables are introduced as in Zukri et al. [20] to solve above equations

$$\zeta = \frac{y}{x}\sqrt{\text{Re}_x}, \psi(x, y) = v_f \sqrt{\text{Re}_x} f(\zeta),$$

$$\theta = \frac{T - T_\infty}{T_w - T_\infty}, \phi = \frac{C - C_\infty}{C_w - C_\infty} \tag{7}$$

where ζ is similarity variable, $\text{Re}_x = \frac{U_\infty x}{v_f}$ refers to Reynolds number, $v_f = \frac{\mu_f}{\rho_f}$ is kinematic viscosity.

Various forms possess distinct numerical shape factors. This shape factor ascertains suitability of shape concerning the nanoparticles. The shape factor, denoted as m in Table 1, together with its numerical values for various forms, is shown in Table 3. The shape factor, m=3/Z, should be acknowledged, where Z represents sphericity. Sphericity being sphere's surface area ratio to particles' surface area with equivalent volumes. Sphericity values for sphere, platelet, cylinder, brick are 1.000, 0.526, 0.625, 0.811, respectively.

Table 1. Thermophysical Relation in Nanoparticles Shape of Hybrid Nanofluids

Properties	Hybrid Nanofluids
Density	$\rho_{hnf} = (1 - \phi_2)\left[(1 - \phi_1)\rho_f + \phi_1\rho_{s1}\right] + \phi_2\rho_{s2}$
Heat Capacity	$(\rho C_p)_{hnf} = (1 - \phi_2)\left[(1 - \phi_1)(\rho C_p)_f + \phi_1(\rho C_p)_{s1}\right] + \phi_2(\rho C_p)_{s2}$
Viscosity	$\mu_{hnf} = \dfrac{\mu_f}{(1 - \phi_1)^{2.5}(1 - \phi_2)^{2.5}}$
Electrical Conductivity	$\sigma_{hnf} = \dfrac{(\sigma_{s2} + 2\sigma_{nf}) - 2\varphi_2(\sigma_{nf} - \sigma_{s2})}{(\sigma_{s2} + 2\sigma_{nf}) + \varphi_2(\sigma_{nf} - \sigma_{s2})} \times \dfrac{(\sigma_{s1} + 2\sigma_f) - 2\varphi_1(\sigma_f - \sigma_{s1})}{(\sigma_{s1} + 2\sigma_f) + \varphi_1(\sigma_f - \sigma_{s1})} (\sigma_f)$

Properties	Hybrid Nanofluids
Thermal Conductivity	$\dfrac{k_{hnf}}{k_{bf}} = \dfrac{k_{s2} + (m-1)k_{bf} - (m-1)\phi_2(k_{bf} - k_{s2})}{k_{s2} + (m-1)k_{bf} - \phi_2(k_{bf} - k_{s2})}$
	$\dfrac{k_{bf}}{k_f} = \dfrac{k_{s1} + (m-1)k_f - (m-1)\phi_1(k_f - k_{s1})}{k_{s1} + (m-1)k_f - \phi_1(k_f - k_{s1})}$
	$k_{bf} = \dfrac{k_{s1} + (m-1)k_f - (m-1)\phi_1(k_f - k_{s1})}{k_{s1} + (m-1)k_f - \phi_1(k_f - k_{s1})} \times k_f$
	$\dfrac{k_{hnf}}{k_f} = \dfrac{k_{hnf}}{k_{bf}} \times \dfrac{k_{bf}}{k_f} = \dfrac{k_{s2} + (m-1)k_{bf} - (m-1)\phi_2(k_{bf} - k_{s2})}{k_{s2} + (m-1)k_{bf} - \phi_2(k_{bf} - k_{s2})} \times \dfrac{k_{s1} + (m-1)k_f - (m-1)\phi_1(k_f - k_{s1})}{k_{s1} + (m-1)k_f - \phi_1(k_f - k_{s1})}$

Table 2. Thermophysical Properties of Base Fluid and Nanoparticles

Properties	Base Fluid (Water)	Ag (Silver)	TiO$_2$ (Titanium Oxide)
$\rho(kg/m^3)$	997.1	10500	4250
$C_p(J/kgK)$	4179	235	686.2
$k(W/mk)$	0.613	429	8.9538

Table 3. Nanoparticles Shape Factors (m)

Nanoparticles Shape	Shapes	Shape Factor (m)	Sphericity (Z)
Spherical		3.0	1.000
Platelets		5.7	0.526
Cylindrical		4.8	0.625
Bricks		3.7	0.811

Following non-linear ODE's result from substituting Eq. (7) into Eqs. (2),(4)

$$\left(1 + \frac{1}{\beta}\right)f''' + A_1\left(ff'' + \gamma\theta + \delta\phi\right) - A_6 A_4 M \sin^2\alpha\left(f' - 1\right) = 0 , \tag{8}$$

$$\left(A_5 + \frac{4}{3}Rd\right)\theta'' + \Pr A_3\left(N_b\theta'\phi' + N_t\theta'^2 + Du\phi'' + f\theta'\right) = 0 , \tag{9}$$

$$\phi'' + ScSr\theta'' + Scf\phi' = 0 . \tag{10}$$

Transformed boundary conditions:

$$\left.\begin{array}{l} f(0) = 0, \ f'(0) = \lambda, \ \theta'(0) = \dfrac{-k_f}{k_{hnf}}\Omega\left(1 - \theta(0)\right) , \phi'(0) = -Bs\left(1 - \phi(0)\right) as \ \zeta = 0, \\[2mm] f'(\zeta) \to 1 \ \theta(\zeta) \to 0, \phi(\zeta) \to 0 \ as \ \zeta \to \infty \end{array}\right\} \tag{11}$$

where:

γ = Thermal Buoyancy parameter $= \frac{Gr_x}{Re_x^2}$, $Gr_x = \dfrac{g\beta_{hnf}(T_w - T_\infty)x^3}{v_f^2}$

δ = Solutal Buoyancy parameter = $\frac{Gc_x}{Re_x^2}$, $Gc_x = \frac{g\beta_{hnf}(C_w - C_\infty)x^3}{v_f^2}$

M = Magnetic parameter = $\frac{B_0^2\sigma_f}{U_\infty\rho_f}$

Pr = Prandtl number = $\frac{v_f(\rho Cp)_f}{k_f}$

Rd = Radiation parameter = $\frac{4\sigma T^3}{k_f k^*}$

N_b = Brownian motion Parameter = $\frac{\tau D_B(C_w - C_\infty)}{v_f}$

N_t = Thermophoresis Parameter = $\frac{\tau D_B(T_w - T_\infty)}{v_f T_\infty}$

Du = Dufour number = $\frac{D_T K_T(C_w - C_\infty)}{v_f C_S C_p(T_w - T_\infty)}$

Sr = Soret number = $\frac{D_T K_T(T_w - T_\infty)}{v_f T_\infty(C_w - C_\infty)}$

Ω = Thermal Biot number = $\frac{h_f}{k_f}\sqrt{\frac{v_f}{U_\infty}}$

Bs = Solutal Biot number = $\frac{h_s}{(D_m)_f}\sqrt{\frac{v_f}{U_\infty}}$

Sc = Schmidt number = $\frac{v_f}{D_m}$

$$A_1 = \left(\frac{\frac{\rho_{hnf}}{\rho_f}}{\frac{\mu_{hnf}}{\mu_f}}\right) = \left((1-\varphi_2)\left[(1-\varphi_1)+\varphi_1\frac{\rho_{s1}}{\rho_f}\right]+\varphi_2\frac{\rho_{s2}}{\rho_f}\right)*\left((1-\varphi_1)^{2.5}(1-\varphi_2)^{2.5}\right)$$

$$A_2 = \left(\frac{\rho_{hnf}}{\rho_f}\right) = = \left((1-\varphi_2)\left[(1-\varphi_1)+\varphi_1\frac{\rho_{s1}}{\rho_f}\right]+\varphi_2\frac{\rho_{s2}}{\rho_f}\right)$$

$$A_3 = \left(\frac{(\rho Cp)_{hnf}}{(\rho Cp)_f}\right) = \left((1-\varphi_2)\left[(1-\varphi_1)+\varphi_1\frac{(\rho Cp)_{s1}}{(\rho Cp)_f}\right]+\varphi_2\frac{(\rho Cp)_{s2}}{(\rho Cp)_f}\right),$$

$$A_4 = \left(\frac{\mu_f}{\mu_{hnf}}\right) = \left((1-\varphi_1)^{2.5}(1-\varphi_2)^{2.5}\right)$$

$$A_5 = \frac{k_{hnf}}{k_f} = \left(\frac{k_{s2}+(m-1)k_{bf}-(m-1)\varphi_2\left(k_{bf}-k_{s2}\right)}{k_{s2}+(m-1)k_{bf}-\varphi_2\left(k_{bf}-k_{s2}\right)}*\frac{k_{s1}+(m-1)k_f-(m-1)\varphi_1\left(k_f-k_{s1}\right)}{k_{s1}+(m-1)k_f-\varphi_1\left(k_f-k_{s1}\right)}\right)$$

$$A_6 = \frac{\sigma_{hnf}}{\sigma_f} = \left(\frac{\sigma_{s2}(1+2\varphi_2)+2\sigma_f(1-\varphi_2)}{\sigma_{s2}(1-\varphi_2)+\sigma_f(2+\varphi_2)}*\frac{\sigma_{s1}(1+2\varphi_1)+2\sigma_f(1-\varphi_1)}{\sigma_{s1}(1-\varphi_1)+\sigma_f(2+\varphi_1)}\right)$$

Skin friction coefficient Cf_x, Heat Transfer Coefficient Nu_x, Sherwood number Sh_x defined as

$$Cf_x = \frac{\tau_w}{\rho_f u_w^2}, \quad Nu_x = \frac{xq_w}{k_f(T_w - T_\infty)}, \quad Sh_x = \frac{xq_m}{D_B(C_w - C_\infty)}$$

$$\tau_w = \mu_{hnf}\left(1+\frac{1}{\beta}\right)\left(\frac{\partial u}{\partial y}\right)_{y=0}, \quad q_w = -k_{hnf}\left(\frac{\partial T}{\partial y}\right)_{y=0}+(q_r)_{y=0}, \quad q_m = -D_B\left(\frac{\partial C}{\partial y}\right)_{y=0}$$

$$q_w = -k_{hnf}\left(\frac{\partial T}{\partial y}\right)_{y=0} + \frac{4\sigma}{3k^*}\frac{\partial T^4}{\partial y},$$

$$Re_x^{1/2} Cf_x = \left(1+\frac{1}{\beta}\right)\left(\frac{f''(0)}{A_4}\right) \tag{12}$$

$$Re_x^{-1/2} Nu_x = -\left(A_5 + \frac{4}{3}Rd\right)\theta'(0) \tag{13}$$

$$Re_x^{-1/2} Sh_x = -\phi'(0) \tag{14}$$

where Re_x is local Reynold's number given by $Re_x = \dfrac{U_\infty x}{v_f}$

NUMERICAL PROCEDURE

To numerically solve the equations according to the boundary conditions, Cebeci and Bradshaw [5] devised an implicit finite difference approach. The necessary actions are as follows:

1. First order equation is created from the converted equations.

2. Central differences are used to write difference equations.

3. Consequently, an algebraic equation is formulated, linearized using Newton's method which is represented as matrix equation.

4. Using Block tri-diagonal elimination approach linear systems is resolved.

Introducing $f' = p$, $p' = q$, $\theta' = t$, $\varphi' = n$

Equations (8),(9), (10) reduced to

$$q' + \left(\frac{\beta}{1+\beta}\right)\left(A_1\left(fq+\gamma\theta+\delta\varphi\right) - A_6 A_4 M \sin^2\alpha\left(p-1\right)\right) = 0 \tag{15}$$

$$\theta'' + \left(\frac{3\Pr A_3}{3A_5 + 4Rd}\right)\left(N_b tn + N_t t^2 + Dufn' + ft\right) = 0 \tag{16}$$

$$n' + ScSrt' + Scfn = 0 \tag{17}$$

Boundary conditions:

$$\left.\begin{array}{l} f = 0, p = \lambda, \Omega\left(1-\theta\right) = -A_5 t, Bs\left(1-\phi\right) = -nas\zeta \to 0 \\ p \to 1, \theta \to 0, \phi \to 0\, as\, \zeta \to \infty \end{array}\right\} \tag{18}$$

RESULTS AND DISCUSSION

Keller Box Method in Matlab numerically enumerates solutions to non-linear ordinary differential equations. To achieve most precise results, it is essential to select and meticulously tune proper initial assumptions optimal boundary layer thickness and various parameter values inside the coding function which covers several variable ranges, including Casson fluid, magnetic fields, buoyancy, thermophoresis, Brownian motion, radiation parameters and Prandtl numbers.

Table 4. Comparing $\theta(0)$, $-\theta'(0)$ results for different Biot number values when M = 0, $\gamma = 0.5$

Ω	Pr = 0.1				Pr = 0.72			
	Aziz[1]		Present study		Aziz[1]		Present study	
	$\theta(0)$	$-\theta'(0)$	$\theta(0)$	$-\theta'(0)$	$\theta(0)$	$-\theta'(0)$	$\theta(0)$	$-\theta'(0)$
5	0.9714	0.1430	0.9703	0.1421	0.9441	0.2791	0.9301	0.2672
10	0.9855	0.1450	0.9848	0.1446	0.9713	0.2871	0.9699	0.2821
20	0.9927	0.1461	0.9928	0.1467	0.9854	0.2913	0.9846	0.2905

To establish the accuracy of our numerical scheme, we first validated our results against the benchmark similarity solution of Aziz [1] for convective boundary-layer flow with constant fluid properties. Table 4 compares surface

temperature $\theta(0)$ and wall heat transfer rate $-\theta'(0)$ for varying Biot numbers at $M = 0, \gamma = 0.5$ Excellent agreement is obtained across all cases, there by confirming the reliability of the Keller Box method employed in this study.

While Aziz [1] restricted attention to Newtonian fluids with constant viscosity and thermal conductivity, the present work extends the formulation in several crucial directions. Unlike Newtonian models, our framework accounts for yield-stress behavior, which is essential in biological and industrial fluids. The combined effects of metal and metal-oxide nanoparticles on transport properties are explored for the first time under cross-diffusion conditions. Our model includes coupled heat-mass transfer phenomena, absent in Aziz's baseline study, which significantly modify thermal and solutal boundary-layer structures. The inclusion of Joule heating, chemical reaction, Brownian motion and variable viscosity/thermal conductivity enables a more realistic representation of actual industrial and biomedical processes.

Certain nanoparticle shapes alter the effective viscosity and flow micro-structure, reducing the momentum boundary layer shear at the surface. The Casson fluid model's shear-thinning property means that with more aligned or elongated nanoparticle shapes, the local resistance to flow can decrease under shear, reducing skin friction.

Increase in heat transfer coefficient depends on thermal conductivity and convective heat transport near wall. Nanoparticle shapes that increase surface area and thermal pathways (e.g., TiO₂ platelets or Ag elongated particles) enhance effective thermal conductivity of nanofluid. Combined with fluid motion either opposing or aiding flow, this increases temperature gradient at wall, raising heat transfer rates.

Figures 2, 3 show skin friction coefficient decreases due to reduction in effective wall shear stress caused by nanoparticle shapes altering the fluid's microstructure and shear-thinning behavior of Casson hybrid nanofluid, especially under relative motion of plate, while heat transfer coefficient increases because these nanoparticle shapes enhance effective thermal conductivity and thermal gradients, improving convective heat transfer despite moving plate conditions.
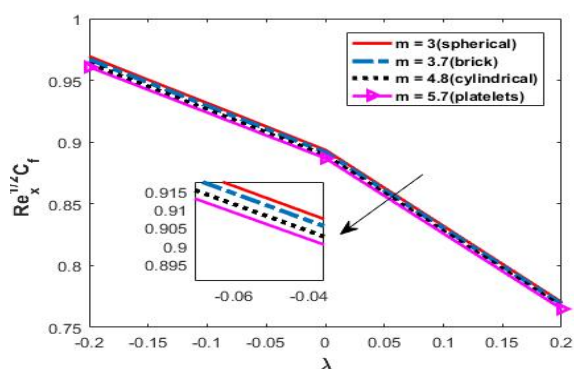

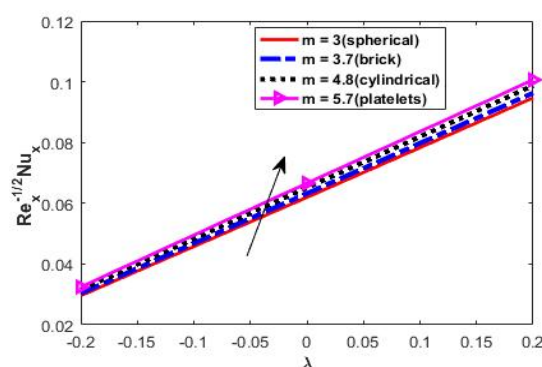**Figure 2. S**kin friction coefficient distribution with variations in m and λ

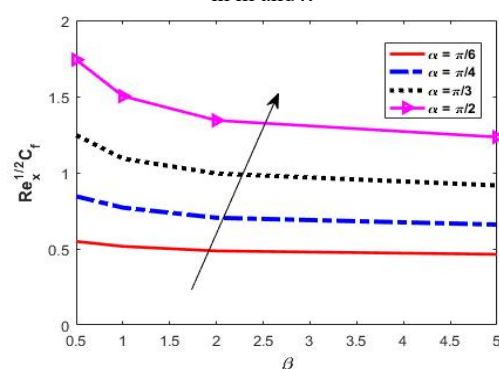**Figure 3.** Heat transfer coefficient distribution with variations in m and λ

Figure 4. Skin friction coefficient distribution with variations in α and β
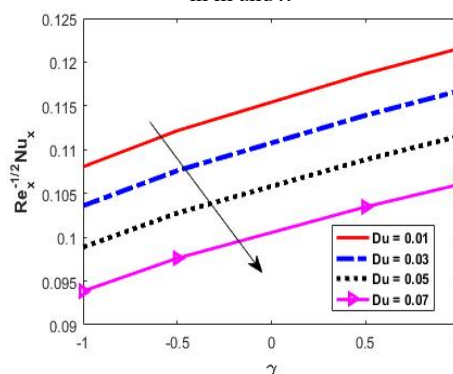

Figure 5. Heat transfer coefficient distribution with variations in γ and Du

In Casson hybrid nanofluids containing silver (Ag) and titanium dioxide (TiO₂) in water, combined effect of an inclined magnetic field, Casson parameter on skin friction coefficient is significant. Figure 4 shows that both parameters contribute to increasing the skin friction. Magnetic field, through Lorentz force, enhances resistance to flow, while Casson parameter, by altering the fluid's rheological properties towards a more Newtonian-like behavior, also increases shear stress at the wall. Numerical studies on Casson hybrid nanofluids often show that the skin friction coefficient increases as these parameters rise. This combined effect underscores the intricate relationship between external fields, fluid rheology and nanoparticle properties in determining the flow characteristics of such complex fluids.

Increasing thermal buoyancy (γ) or Dufour number adds extra velocity into the boundary layer, making it thicker and less steep near the wall, thereby lowering the wall temperature gradient and reducing the heat transfer coefficient distribution as shown in Figure 5.

When buoyant forces resulting from heat or concentration gradients are substantial, the inclined magnetic field can interact with these forces to augment flow velocity. Tilt of magnetic field can modify direction, intensity of buoyancy-driven flows, occasionally resulting in enhanced convective currents and elevated velocity profiles as shown in Figure 6. Figure 7 shows that temperature profiles diminish with a rise in the inclined magnetic field, since the magnetic field inhibits fluid mobility, hence decreasing convective heat transfer and leading the fluid to retain less thermal energy at heated surface. Inclined magnetic field often inhibits nanoparticle motion, diminishing thickness of concentration boundary layer and decreasing concentration profiles shown in Figure 8.
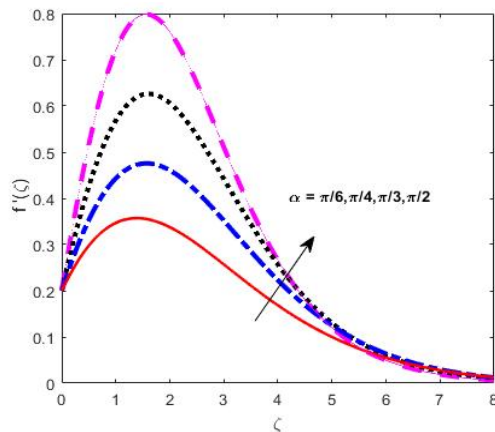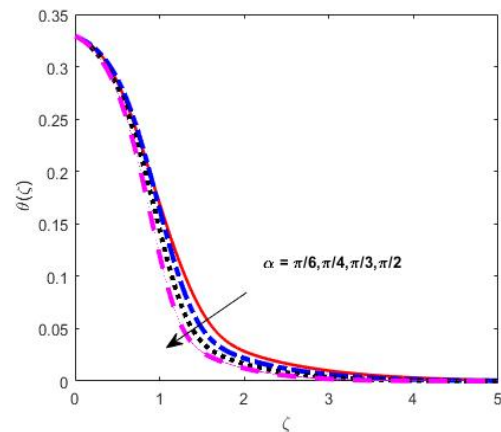
Figure 6. Velocity $f'(\zeta)$ versus α
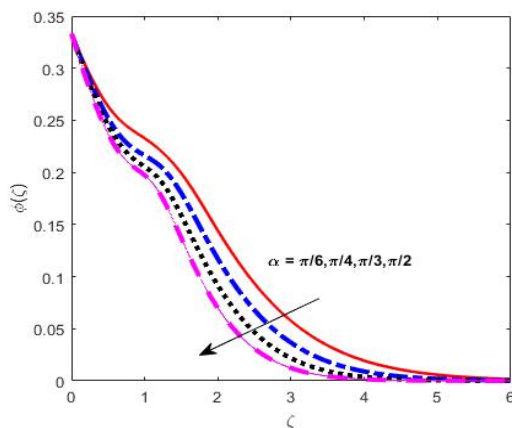
Figure 7. Temperature $\theta(\zeta)$ versus α

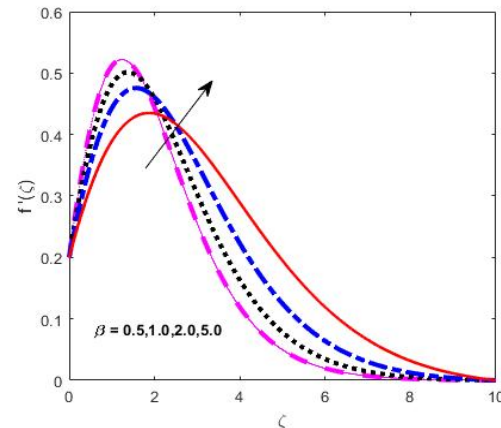**Figure 8.** Concentration $\varphi(\zeta)$ versus α

Figure 9. Velocity $f'(\zeta)$ versus β

Figure 9 demonstrates that elevating Casson parameter often diminishes fluid velocity next to the channel walls, owing to the augmented fluid yield stress that impedes flow start and lessens velocity gradients at the boundaries. The reduction in temperature profiles with an increasing Casson parameter as shown in Figure 10, is mostly attributed to augmented flow resistance and diminished convective heat transfer caused by the fluid's non-Newtonian rheology. Figure 11 shows the diminished nanoparticle concentration profiles adjacent to the walls, as the fluid's augmented resistance to flow restricts mass transfer and curtails nanoparticle movement into boundary layers.
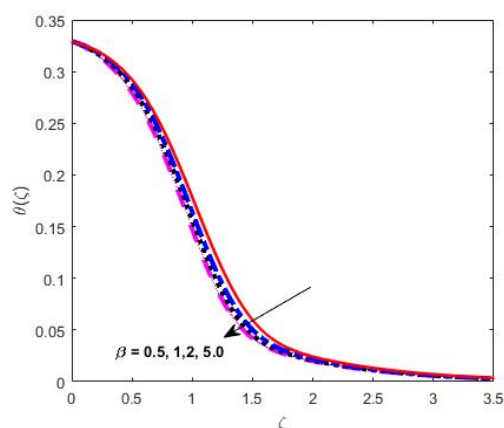
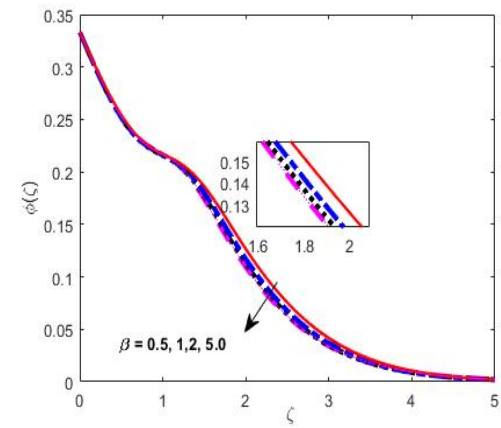**Figure 10.** Temperature $\theta(\zeta)$ versus β
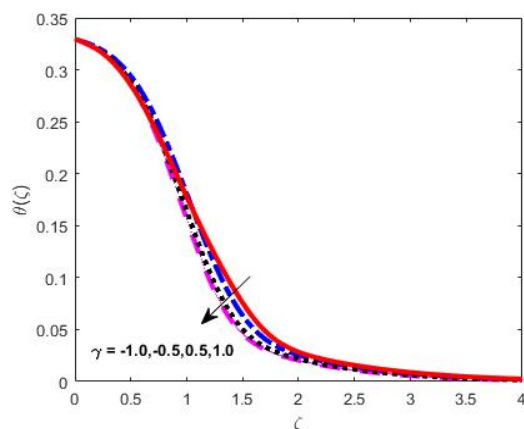
Figure 11. Concentration $\varphi(\zeta)$ versus β

Figure 12. Temperature $\theta(\zeta)$ versus γ
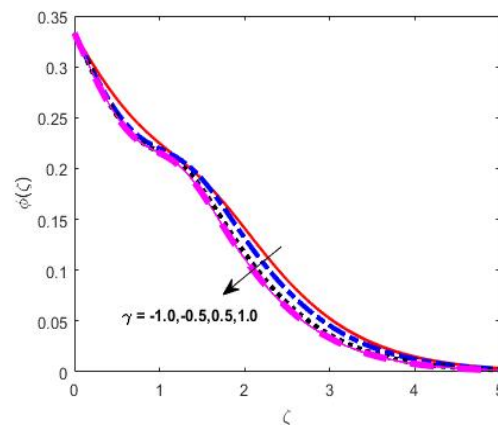
Figure 13. Concentration $\varphi(\zeta)$ versus γ
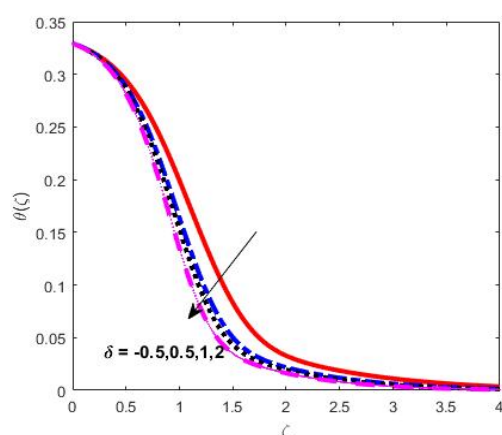
Figure 14. Temperature $\theta(\zeta)$ versus δ

Figure 15. Concentration $\varphi(\zeta)$ versus δ

Figure 12 shows a counterintuitive decrease in temperature profile with higher thermal buoyancy parameter in Casson hybrid nanofluids with Ag and TiO$_2$ arises mainly due to enhanced natural convection and fluid mixing that accelerate heat removal from heated surfaces, thinning the thermal boundary layer and reducing local temperatures near those surfaces. The concentration profile typically shows a decrease as shown in Figure 13, with increasing thermal buoyancy parameter as the enhanced upward movement of fluid transports nanoparticles and dissolved substances away from heated surfaces, thinning the concentration boundary layer.

The temperature profile typically declines as the solutal buoyancy parameter increases, since enhanced solutal buoyancy intensifies mixing and convective transport, hence diminishing heat gradients near the surface, the reduction in concentration profiles with an increasing solutal buoyancy parameter as shown in Figures 14 and 15,results from intensified buoyancy forces that augment convective mass transfer away from wall, thereby diminishing nanoparticle concentration in boundary layer of the Casson hybrid nanofluid comprising silver and TiO₂ in water.
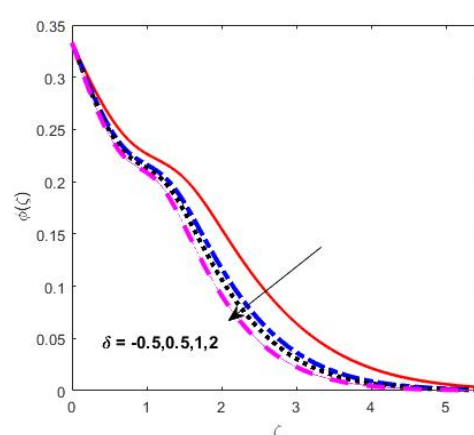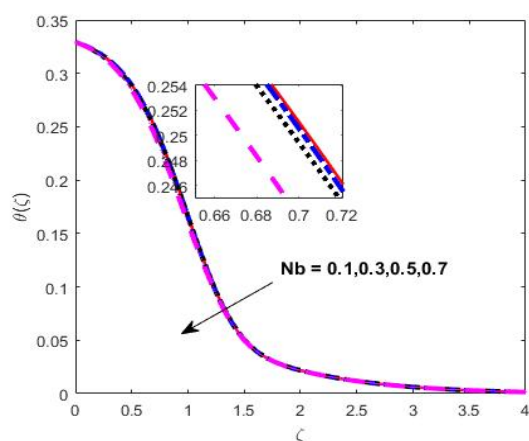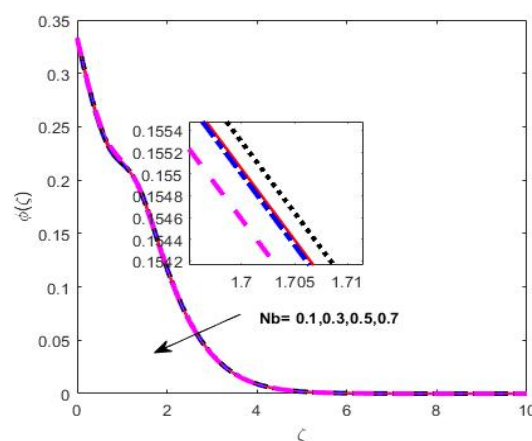

Figure 16. Temperature $\theta(\zeta)$ versus Nb

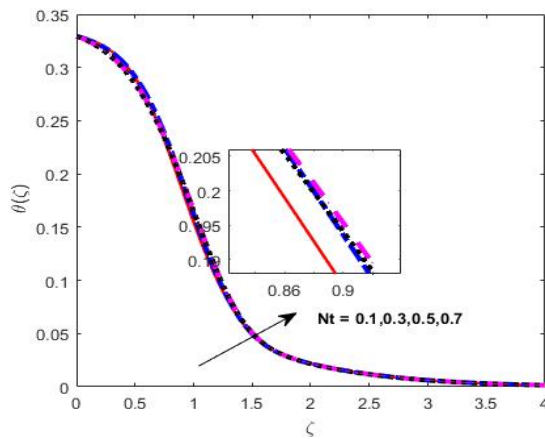**Figure 17.** Concentration $\varphi(\zeta)$ versus Nb

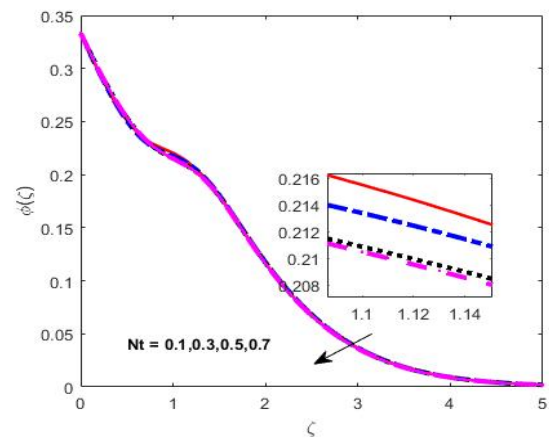**Figure 18.** Temperature $\theta(\zeta)$ versus Nt

Figure 19. Concentration $\varphi(\zeta)$ versus Nt

Figure 16, 17 demonstrates temperature, concentration profiles decrease with increasing Brownian motion parameter as its enhancement intensifies nanoparticle diffusion, which reduces the concentration gradient by dispersing nanoparticles more effectively. This also disturbs thermal boundary layer by increasing heat dispersion, decreasing effective nanoparticle concentration near the surface, leading to thinner thermal, concentration boundary layers in Casson hybrid nanofluid containing Ag and TiO_2 nanoparticles suspended in water.

Figure 18 shows that as the thermophoresis parameter increases, temperature profiles rise due to enhanced thermal transport mechanisms within the hybrid nanofluid. This increase in temperature promotes greater kinetic energy among the particles. Conversely, the concentration profiles decrease because thermophoretic effect causes particles to migrate away from higher temperature regions leading to reduction in concentration as shown in Figure 19.
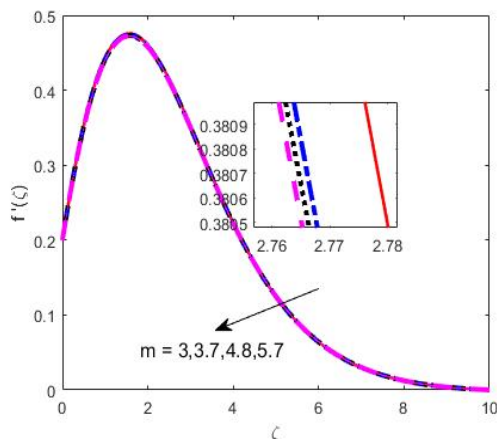
Figure 20. Velocity $f'(\zeta)$ versus m

Figure 21. Temperature $\theta(\zeta)$ versus m
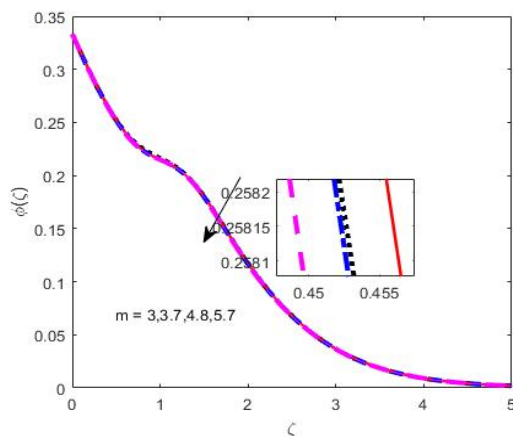
Figure 22. Concentration $\varphi(\zeta)$ versus m
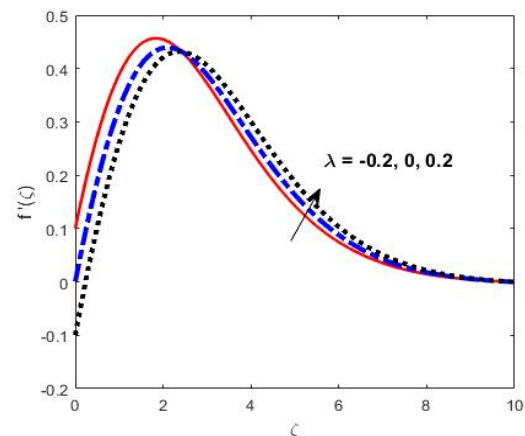
Figure 23. Velocity $f'(\zeta)$ versus λ

Figures 20, 21 and 22 demonstrates the influence of nanoparticle shape factor.Increasing nanoparticle shape factor in Ag-TiO2 hybrid nanofluids increases viscosity and flow resistance. These effects lower fluid velocity profiles,

especially at solid boundaries or surfaces where particle-fluid interactions and viscous forces are most significant. Complex flow dynamics, such as magnetic field impacts and boundary layer alterations, further reduce velocity. Hybrid nanofluid temperature profiles drop as nanoparticle shape factor rises, reaching a minimum and then slightly rising for disk nanoparticles. Thermal disturbance and heat transmission are better in spherical nanoparticles. Blade-shaped nanoparticles transmit heat fastest, followed by cylindrical, platelet, brick, and spherical forms. Because nanoparticle morphology improves dispersion and convective mass transfer, Ag-TiO2 hybrid nanofluid concentration profiles drop with nanoparticle shape factor. More uniform nanoparticle dispersion, thinner boundary layer, and smaller local concentration peaks result. This behavior is governed by micro-convection, fluid mixing, viscosity variations, and shape-factor-driven thermophoretic mass flow.
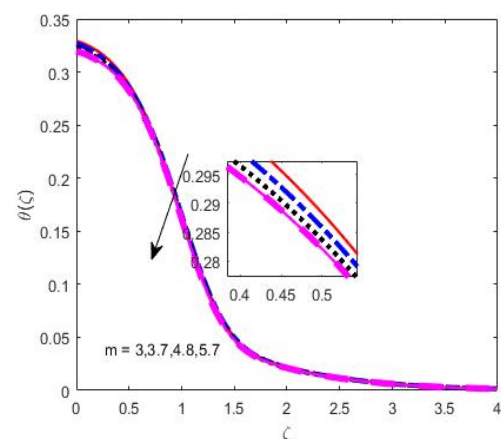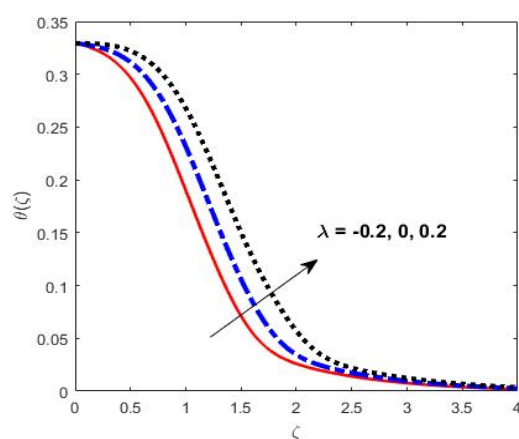

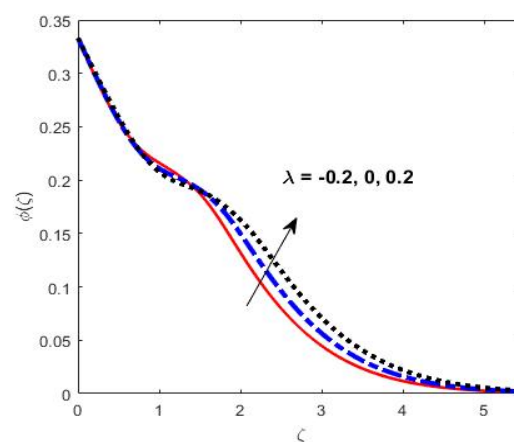**Figure 24.** Temperature $\theta(\zeta)$ versus λ

Figure 25. Concentration $\varphi(\zeta)$ versus λ

Figures 23, 24 and 25 demonstrates the effect of moving plate parameter. The momentum boundary layer thickens as the plate moves in the flow direction, while velocity profiles drop as it goes against the flow. Convective heat transfer from the moving plate raises nearby temperatures. Increasing nanoparticle dispersion with parameters like thermophoresis raises temperature. Nanoparticle transport increases mass diffusion and thins the concentration boundary layer with plate motion in the flow direction. This reduces nanoparticle concentration near the plate as particles are swept downstream, enhancing distribution uniformity.

Figure 26 shows that with elevation in the solutal Biot number often improves the temperature distribution in the hybrid nanofluid. This arises from the solutal Biot number, which quantifies convective to diffusive mass transfer resistance. Concentration profiles of nanoparticles or solutes in the hybrid nanofluid escalate with the solutal Biot number. A greater solutal Biot number signifies improved convective mass movement at the surface, which decreases concentration boundary layer thickness and increases solute or nanoparticle concentration near boundary. Consequently, concentration boundary layers diminish in thickness and concentration gradients intensify as solutal Biot number increases as shown in figure 27.
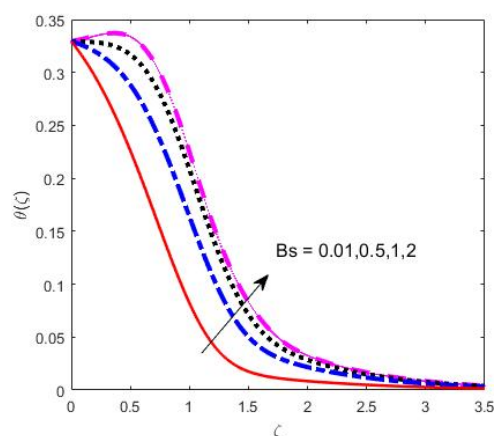
Figure 26. Temperature $\theta(\zeta)$ versus Bs
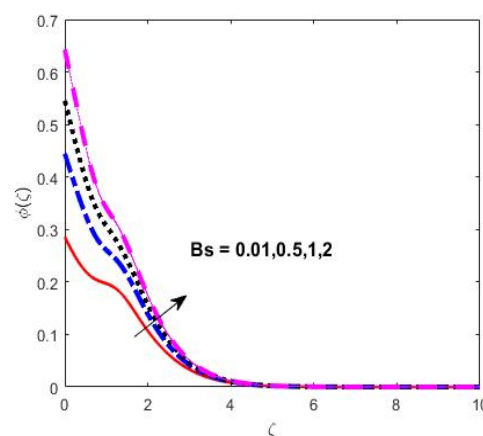
Figure 27. Concentration $\varphi(\zeta)$ versus Bs

Temperature profile improves with higher thermal Biot numbers as shown in figure 28. The thermal Biot number is surface convective to fluid conductive heat transfer ratio. Higher Biot numbers imply more convective heat exchange between fluid, its surroundings resulting in thicker thermal boundary layers, higher fluid temperatures near surface. Better heat transfer and local Nusselt values indicate more efficient thermal energy delivery. The hybrid nanofluid system's thermal radiation, heat source intensity, and Brownian motion boost temperature distribution. The heat

transmission coefficient increases with Biot number, creating a greater temperature differential and higher fluid temperatures near the heated surface. Figure 29 shows thermal Biot number increases concentration dispersion, however Schmidt number and chemical reaction rates can mitigate this impact. The concentration boundary layer thickness and form depend on this interaction.

Figure 28. Temperature $\theta(\zeta)$ versus Ω
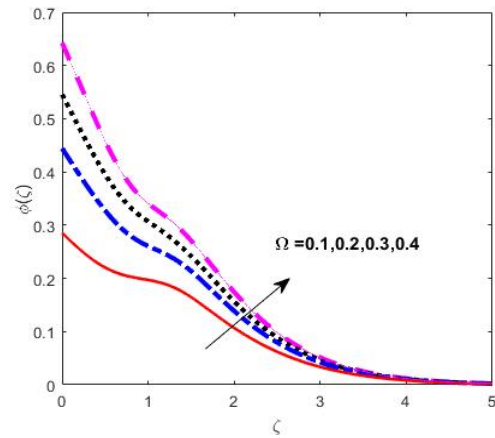
Figure 29. Concentration $\varphi(\zeta)$ versus Ω

Dufour effect represents the heat flux generated by concentration gradients within fluid. In Casson hybrid nanofluids with Ag and TiO2 nanoparticles, this effect leads to increase in temperature profile near surface because heat transfer is augmented by mass diffusion processes. As the Dufour number increases, more heat is transported into the fluid from concentration gradients, thereby elevating the fluid temperature as shown in Figure 30.

The Soret effect causes species within the nanofluid to migrate from colder to hotter regions due to temperature gradients, resulting in enhanced concentration gradients. In Casson hybrid nanofluids with Ag and TiO2 nanoparticles, this leads to an increase in nanoparticle concentration near the heated surfaces as shown in Figure 31 enriching the solute distribution in the fluid.
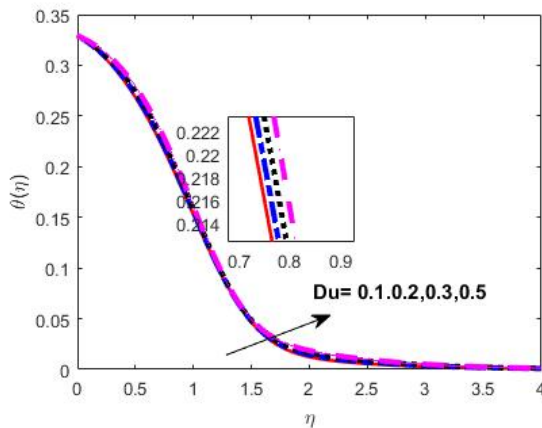
Figure 30. Temperature $\theta(\zeta)$ versus Du
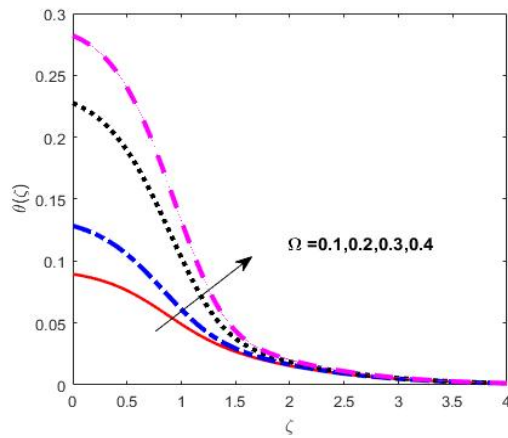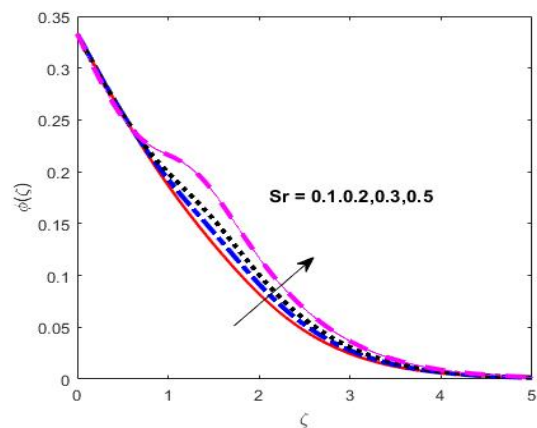

Figure 31. Concentration $\varphi(\zeta)$ versus Sr

Tables 5,6 and 7 below shows variation in skin friction coefficient, Nusselt number, Sherwood number for various nanoparticle shapes when plate moves in accordance with flow. From tabulated values, spherical shape shows highest skin friction, Sherwood number for all parameters whereas platelet shape has highest nusselt number for increasing Biot number.

Table 5. Variation in Skin Friction Coefficient f'(0)

α	M	φ₁	φ₂	βc	Skin Friction $f''(0)$			
					Shapes of nanoparticles			
					Spherical	Bricks	Cylindrical	Platelets
0°	1	0.1	0.1	2	0.400115	0.393619	0.385249	0.379654
30°					0.623173	0.615313	0.605506	0.599195
60°					1.338845	1.331604	1.322577	1.316769
90°					1.831634	1.824847	1.816386	1.810939
90°	0				0.400115	0.393619	0.385249	0.379654
	1				1.831634	1.824847	1.816386	1.810939
	2				4.500536	4.495191	4.488521	4.484220
	3				8.017072	8.012569	8.006946	8.003315

α	M	φ_1	φ_2	β_c	Skin Friction $f''(0)$			
					Shapes of nanoparticles			
					Spherical	Bricks	Cylindrical	Platelets
1	1	0	0		1.213740	1.213740	1.213740	1.213740
		0	0.1		1.606387	1.604808	1.602760	1.601382
		0.1	0		1.280598	1.277597	1.273458	1.270503
		0.05	0.05		1.406770	1.404328	1.400976	1.398591
		0.1	0.1	1	2.034106	2.028023	2.020232	2.015055
				2	1.831634	1.824847	1.816386	1.810939
				5	1.684668	1.678128	1.669972	1.664721
				100	1.579132	1.572756	1.564803	1.559681

Table 6. Variation in Nusselt number θ'(0)

Rd	N_b	N_t	Du	γ	Ω	Nusselt Number $\theta'(0)$			
						Shapes of nanoparticles			
						Spherical	Bricks	Cylindrical	Platelets
1	0.3	0.3	0.1	0.5	0.1	0.090411	0.089705	0.088655	0.087842
2						0.138606	0.137220	0.135167	0.133588
3						0.180374	0.178423	0.175541	0.173327
5						0.251698	0.248818	0.244566	0.241304
1	0.1					0.090398	0.089692	0.088642	0.087830
	0.3					0.090411	0.089705	0.088655	0.087842
	0.5					0.090424	0.089719	0.088668	0.087855
	0.7					0.090438	0.089733	0.088682	0.087869
		0.1				0.090409	0.089703	0.088653	0.087841
		0.3				0.090411	0.089705	0.088655	0.087842
		0.5				0.090412	0.089707	0.088657	0.087844
		0.7				0.090414	0.089709	0.088658	0.087846
	0.3	0.3	0.01			0.114346	0.113732	0.112819	0.112114
			0.03			0.109277	0.108642	0.107699	0.106948
			0.05			0.104057	0.103402	0.102429	0.101676
			0.07			0.098705	0.098030	0.097026	0.096249
				-0.5		0.089477	0.088785	0.087756	0.086958
				-1.0		0.089000	0.088316	0.087297	0.086508
				0.5		0.090411	0.089705	0.088655	0.087842
				1.0		0.090857	0.090145	0.089085	0.088265
				0.5	0.5	0.315639	0.315791	0.315988	0.316117
					1	0.411254	0.412808	0.415106	0.416874
					5	0.515960	0.520103	0.526355	0.531266
					10	0.529210	0.533793	0.540726	0.546186

Table 7. Variation in Sherwood number φ'(0):

β_c	δ	Bs	Sc	Sr	Sherwood Number $\varphi'(0)$			
					Shapes of nanoparticles			
					Spherical	Bricks	Cylindrical	Platelets
1	0.5	0.5	1.0	0.5	0.181278	0.181111	0.180871	0.180694
2					0.184588	0.184427	0.184197	0.184027
5					0.186499	0.186348	0.186132	0.185973
100					0.187395	0.187253	0.187053	0.186906
1	-0.5				0.172397	0.172250	0.172041	0.171886
	0.5				0.181278	0.181111	0.180871	0.180694
	1				0.185024	0.184848	0.184597	0.184411
	2				0.188765	0.188596	0.188354	0.188175
		0.5			0.181278	0.181111	0.180871	0.180694
		1			0.292474	0.292205	0.291813	0.291516
		2			0.403236	0.402890	0.402382	0.401994
		10			0.563659	0.563238	0.562617	0.562140
	0.5		0.5		0.127680	0.127661	0.127638	0.127624
			1.0		0.181278	0.181111	0.180871	0.180694
			1.5		0.227563	0.227176	0.226614	0.226192
			2.0		0.272782	0.272107	0.271122	0.270376
		0.5	1.0	0.1	0.190251	0.190201	0.190128	0.190073
				0.2	0.188187	0.188108	0.187994	0.187909

β_c	δ	Bs	Sc	Sr	Sherwood Number $\varphi'(0)$			
					Shapes of nanoparticles			
					Spherical	Bricks	Cylindrical	Platelets
				0.3	0.186013	0.185905	0.185750	0.185634
				0.5	0.181278	0.181111	0.180871	0.180694

CONCLUSIONS

Casson hybrid nanofluid flow along plate moving vertically with Soret, Dufour effects considering nanoparticles shapes were investigated in this study. Convective boundary conditions were also considered. Following are findings of this research:

i.   Temperature and concentration distribution drop and velocity outline rises with increase in inclination parameter.

ii. Velocity increases while temperature and concentration show an opposite trend, as Casson parameter rises,

iii. Mass diffusion and fluid energy decrease by boosting the Brownian motion factor.

iv. Temperature profile is elevated by thermophoresis factor, while concentration is lowered.

v.   Temperature and concentration also increase, with rise in Bs and Ω,

vi. Temperature and concentration show a fall in their profiles, when thermal buoyancy and solutal buoyancy parameters are modified,

vii. Platelet shaped nanoparticle was shown to have highest velocity, temperature, concentration profiles followed by cylindrical, bricks, spherical shape.

viii. Skin friction coefficient increases with increase in β values when magnetic field is applied perpendicularly.

ix. Platelet shaped nanoparticle has highest skin friction when plate moves against flow, while plate moving in accordance with flow gives highest Nusselt number.

Conflict of Interest & Acknowledgement

Nomenclature

U	Characteristic velocity of the moving plate(m/s)		**Greek Symbols**	
x,y	Cylindrical coordinates (m)	β	Casson Parameter	
k	Thermal conductivity of the fluid (W/mK)	λ	Moving plate parameter	
T_w	Plate temperature (K)	γ	Thermal Buoyancy parameter	
T_∞	Ambient temperature (K)	δ	Solutal Buoyancy parameter	
C_w	Plate concentration(kg/m^3)	ζ	Similarity variable	
C_∞	ambient concentration(kg/m^3)	τ_w	Wall shear stress (kg/ms^2)	
Nu_x	Nusselt Number	ρ	Density of the fluid (kg/m^3)	
Re_x	Reynolds number	C_p	Specific heat at constant pressure (J/kgK)	
Sh_x	Sherwood number	ρC_p	Heat capacitance of fluid (J/Km^3)	
C_{fx}	skin friction coefficient	α	Thermal diffusivity(m^2/s)	
Ω	Thermal Biot number	σ	Electrical conductivity(S/m)	
Bs	SolutalBiot number	μ	Dynamic viscosity of the fluid (kg/ms)	
Sr	Soret effect	υ_f	Kinematic viscosity of the fluid (m^2/s)	
Du	Dufour effect			
M	Magnetic field parameter		**Superscripts**	
Pr	Prandtl number	'	differentiation with respect to h	
K	Porosity parameter			
Rd	Radiation parameter		**Subscripts**	
N_b	Brownian motion Parameter	f	fluid	
N_t	Thermophoresis Parameter	nf	nanofluid	
Sc	Schmidt number	hnf	Hybrid nanofluid	

ORCID

K. Fatima, https://orcid.org/0009-0007-5459-1773; **J.L. Rama Prasad,** https://orcid.org/0000-0003-3604-5182

REFERENCES

[1] A. Aziz, "A similarity solution for laminar thermal boundary layer over a flat plate with a convective surface boundary condition," Commun. Nonlinear Sci. Numer. Simulat. **14**, 1064-1068 (2009). https://doi.org/10.1016/j.cnsns.2008.05.003

[2] A. Yahyaee, "Influence of nanoparticle shapes in nanofluid film boiling on vertical cylinders: A numerical study," International Journal of Thermofluids, **22**, 100631 (2024). https://doi.org/10.1016/j.ijft.2024.100631

[3] A. Hussain, S. Raiz, A. Hassan, A.M. Hassan, H. Karamti, and G. Bognár, "Analysis of Soret and Dufour effects on radiative heat transfer in hybrid bioconvective flow of carbon nanotubes," Scientific Reports**,** (2024). https://doi.org/10.1038/s41598-024-62647-2

[4]   B.N. Lakshmi, V.S. Bhagavan, M.R. Ravuri, and G.V.R. Reddy, "Contribution of Soret and Dufour aspects on Hybrid Nanofluid over 3D Magneto Radiative Stretching Surface with Chemical Reaction," CFD Letters, **17**(5), 131-151 (2025). https://doi.org/10.37934/cfdl.17.5.131151

[5]   Cebeci and Bradshaw, *A Physical and Computational Aspects of Convective Heat transfer*, (Springer-Verlag, New York,1988).

[6]   Ch. RamReddy, P.V.S.N. Murthy, A.J. Chamkha, and A.M. Rashad, "Soret effect on mixed convection flow in a nanofluid under convective boundary condition," International Journal of Heat and Mass Transfer, **64**, 384-392 (2013). https://doi.org/10.1016/j.ijheatmasstransfer.2013.04.032

[7]   C. Maheswari, R.M. Ramana, G.B. Prakash, D. Ramesh, and D.V. Kumar, "Influence of Thermophoresis and Brownian Motion on MHD Hybrid Nanofluid MgO - Ag/H2O Flow along Moving Slim Needle," Journal of Advanced Research in Applied Sciences and Engineering Technology, **36**(2), 67-90 (2024). https://doi.org/10.37934/araset.36.2.6790

[8]   E. Seid, E. Haile, and T. Walelign, "Multiple slip, Soret and Dufour effects in fluid flow near a vertical stretching sheet in the presence of magnetic nanoparticles," International Journal of Thermofluids, **13**, 100136 (2022). https://doi.org/:10.1016/j.ijft.2022.100136

[9]   S.S.P.M. Isa, S. Parvin, N.M. Arifin, F.M. Ali, and K. Ahmad, "Soret-Dufour Effects on The Water based Hybrid Nanofluid Flow with Nanoparticles of Alumina and Copper," Malaysian Journal of Mathematical Sciences, **17**(3), 283–304 (2023). https://doi.org/10.47836/mjms.17.3.04

[10] I. Waini, A. Ishak, T. Groşan, and I. Pop, "Mixed convection of a hybrid nanofluid flow along a vertical surface embedded in a porous medium," International Communications in Heat and Mass Transfer, **114**, 104565 (2020). https://doi.org/10.1016/j.icheatmasstransfer.2020.104565

[11] J. Jayaprakash, V. Govindan, S.S. Santra, S.S. Askar, A. Foul, S. Nandi, S.M. Hussain, "Thermal radiation, Soret and Dufour effects on MHD mixed convective Maxwell hybrid nanofluid flow under porous medium: a numerical study," International Journal of Numerical Methods for Heat & Fluid Flow, **34**(10), 3924-3952 (2024). https://doi.org/10.1108/HFF-03-2024-0229

[12] K. Jat, K. Sharma, P. Soni and P. Choudhary, "Numerical analysis of heat and mass transport of hybrid nanofluid over a nonlinear stretchable sheet with magnetic field in presence of Soret and Dufour Effect," Journal of Physics: Conference Series, **2844**, 012019 (2024). https://doi.org/10.1088/1742-6596/2844/1/012019

[13] K.S. Balamurugan, J.L. Ramaprasad, D. Gurram, and V.C.C. Raju, "Influence of Radiation Absorption, Viscous and Joules dissipation on MHD free Convection Chemically Reactive and Radiative Flow in a Moving Inclined Porous Plate with Temperature Dependent Heat Source," International Refereed Journal of Engineering and Science, **5**(12), 20-31 (2016).

[14] M.A. Adriana, "Hybrid nanofluids based on Al2O3, TiO2 and SiO2: Numerical evaluation of different approaches," International Journal of Heat and Mass Transfer, **104**, 852–860 (2017). https://doi.org/10.1016/j.ijheatmasstransfer.2016.09.012

[15] M.A. Mansour, and M.A.Y. Bakier, "Magnetohydrodynamic mixed convection of TiO2-Cu/water between the double lid-driven cavity and a central heat source surrounding by a wavy tilted domain of porous medium under local thermal non-equilibrium," S.N. Applied Sciences, **5**, 51 (2023). https://doi.org/10.1007/s42452-022-05260-0

[16] M. Sheikholeslami, M.M. Bhatti, "Forced convection of nanofluid in presence of constant magnetic field considering shape effects of nanoparticles," International Journal of Heat and Mass Transfer, **111**, 1039–1049 (2017). https://doi.org/10.1016/j.ijheatmasstransfer.2017.04.070

[17] M.S. Babu, V.V. Ramana, G.R. Shankar, and C.S.K. Raju, "Mixed convective flow of heat and mass transfer of nanofluids over a static wedge with convective boundary conditions," Journal of Thermal Engineering, **7**(14), 1958–1969 (2021). https://doi.org/10.18186/thermal.1051302

[18] M.V. Krishna, N.A. Ahammad, and A.J. Chamkha, "Radiative MHD flow of Casson hybrid nanofluid over an infinite exponentially accelerated vertical porous surface," Case Studies in Thermal Engineering, **27**, 101229 (2021). https://doi.org/10.1016/j.csite.2021.101229

[19] N.A. Rosaidi, N.H. AbRaji, S.N. Hidayatu, A. Ibrahim, and M.R. Ilias, "Aligned Magnetohydrodynamics Free Convection Flow of Magnetic Nanofluid over a Moving Vertical Plate with Convective Boundary Condition," Journal of Advanced Research in Fluid Mechanics and Thermal Sciences, **93**(2), 37-49 (2022). https://doi.org/10.37934/arfmts.93.2.3749

[20] N.Z.M. Zukri, M.R. Ilias, S.S. Ishak, R. Osman, N.A.M. Makhatar, and M.N. AbdRahman, "Magnetohydrodynamic Effect in Mixed Convection Casson Hybrid Nanofluids Flow and Heat Transfer over a Moving Vertical Plate," CFD Letters, **15**(7), 92-111 (2023). https://doi.org/10.37934/cfdl.15.7.92111

[21] N.S. Akbar, and A.W. Butt, "Ferromagnetic effects for peristaltic flow of Cu–water nanofluid for different shapes of nanosize particles," Applied Nanoscience, 6, 379–385 (2016). https://doi.org/10.1007/s13204-015-0430-x

[22] N.A. Zainal, R. Nazar, K. Naganthran, and I. Pop, "MHD mixed convection stagnation point flow of a hybrid nanofluid past a vertical flat plate with convective boundary condition," Chinese Journal of Physics, **66**, 630–644 (2020). https://doi.org/10.1016/j.cjph.2020.03.022

[23] P. Chandrakala, and V.S. Rao, "Effect of Heat and Mass Transfer over Mixed Convective Hybrid Nanofluids past an Exponentially Stretching Sheet," CFD Letters, **16**(3),125-140 (2024). https://doi.org/10.37934/cfdl.16.3.125140

[24] R. Jain, R. Mehta, A. Bhatnagar, H. Ahmad, Z.A. Khan, and G.M. Ismail, "Numerical study of heat and mass transfer of Williamson hybrid nanofluid (CuO/CNT's-water) past a permeable stretching/shrinking surface with mixed convective boundary condition," Case Studies in Thermal Engineering, **59**, 104313 (2024). https://doi.org/10.1016/j.csite.2024.104313

[25] S. Goudarzi, M. Shekaramiz, A. Omidvar, E. Golab, A. Karimipour, and A. Karimipour, "Nanoparticles migration due to thermophoresis and Brownian motion and its impact on Ag-MgO/Water hybrid nanofluid natural convection," Powder Technology, **375**, 493–503 (2020). https://doi.org/10.1016/j.powtec.2020.07.115

[26] S.A.M. Mehryan, F.M. Kashkooli, M. Ghalambaz, and A.J. Chamkha, "Free convection of hybrid Al2O3-Cu water nanofluid in a differentially heated porous cavity," Advanced Powder Technology, **28**(9), 2295-2305 (2017). https://doi.org/10.1016/j.apt.2017.06.011

[27] S. Hussain, K. Mehmood, and M. Sagheer, "MHD mixed convection and entropy generation of water–alumina nanofluid flow in a double lid driven cavity with discrete heating," Journal of Magnetism and Magnetic Materials, **419**, 140–155 (2016). https://doi.org/10.1016/j.jmmm.2016.06.006

[28] T. Anwar, P. Kumam, and P. Thounthong, "A comparative fractional study to evaluate thermal performance of NaAlg-MoS2-Co hybrid nanofluid subject to shape factor and dual ramped conditions," Alexandria Engineering Journal, **61**, 2166–2187 (2022). https://doi.org/10.1016/j.aej.2021.06.085

[29] T.S. Khaleque, A. Hossain, M.D. Shamshuddin, M. Ferdows, S.O. Salawu, and S. Sun, "Soret and Dufour impacts on radiative power-law fluid flow via continuously stretchable surface with varying viscosity and thermal conductivity," Scientific Reports, **14**, 23152 (2024). https://doi.org/10.1038/s41598-024-73426-4

ЕФЕКТИ СОРЕ ТА ДЮФУРА НА Ag–ТІО₂/ВОДА В ГІБРИДНІЙ НАНОРІДИНІ КЕССОНА НАД РУХОМОЮ ВЕРТИКАЛЬНОЮ ПЛАСТИНКОЮ З КОНВЕКТИВНИМИ ГРАНИЧНИМИ УМОВАМИ

К. Фатіма[1], Дж.Л. Рама Прасад[2]
[1]Кафедра математики, Університет Крішни, Мачіліпатнам, АР, Індія
[2]Кафедра математики, Коледж мистецтв і наук ім. П.Б. Сіддхартхи, Віджаявада, АР, Індія

Це дослідження представляє комплексне дослідження ефектів Соре та Дюфура на потік гібридної нанорідини Кассона (HNF) повз рухому вертикальну пластину з наночастинками срібла (Ag) та діоксиду титану (TiO₂), диспергованими у воді. Включення гібридних наночастинок Ag–TiO₂ поєднує виняткову теплопровідність срібла з хімічною стабільністю та економічною ефективністю TiO₂, створюючи рідину з чудовими транспортними властивостями порівняно зі звичайними однокомпонентними нанорідинами. Визначальні диференціальні рівняння в частинних похідних, що описують імпульс, тепло- та масообмін, перетворюються на набір нелінійних звичайних диференціальних рівнянь за допомогою перетворень подібності. Ці рівняння розв'язуються чисельно за допомогою методу Келлер-Бокса, що забезпечує стабільність і точність при роботі зі зв'язаними високонелінійними системами. Крім того, було проведено аналіз для вивчення впливу морфології наночастинок на розподіл швидкості, температури та концентрації, що підтверджує та збагачує числові результати. Результати показують, що змінна морфологія наночастинок та комбінована дисперсія Ag-TiO₂ значно підвищують швидкість теплопередачі та масообміну, одночасно зменшуючи втрати на тертя поблизу поверхні пластини. Включення ефектів Соре та Дюфура ще більше посилює перехресний зв'язок між тепловими та розчинними полями, що призводить до підвищення ефективності переносу. Ці результати не тільки дають нове розуміння динаміки гібридних нанорідин Кассона, але й підкреслюють критичну роль перехресної дифузії в оптимізації систем тепло- та масообміну. Інтеграція реології рідини Кассона, гібридних наночастинок та ефектів перехресної дифузії в реалістичних граничних умовах має прямі наслідки для промислового охолодження, металургійної обробки, доставки біомедичних ліків та оптимізації енергетичних систем. Демонструючи синергетичну ефективність нанорідин Ag–TiO₂, це дослідження встановлює шлях для розробки технологій терморегуляції та біомедичного транспорту наступного покоління.

Ключові слова: *конвективні граничні умови; МГД; гібридна нанорідина Кассона; форма наночастинок; ефекти Соре та Дюфура*